JACS
JOURNAL OF THE AMERICAN CHEMICAL SOCIETY

Article

pubs.acs.org/JACS

Raman Spectroscopy Reveals Selective Interactions of Cytochrome *c* with Cardiolipin That Correlate with Membrane Permeability

Jay P. Kitt, David A. Bryce, Shelley D. Minteer, and Joel M. Harris*

Department of Chemistry, University of Utah, 315 South 1400 East, Salt Lake City, Utah 84112, United States

Supporting Information

ABSTRACT: Permeabilization of the outer mitochondrial membrane is an integral step in apoptosis. The resulting release of pro-apoptotic signaling proteins leads to cell destruction through activation of the cysteine-aspartic protease (caspase) cascade. However, the mechanism of outer mitochondrial membrane (OMM) permeabilization remains unclear. It was recently shown that cytochrome *c* can induce pore formation in cardiolipin-containing phospholipid membranes, leading to large dextran and protein permeability. In this work, the interaction of cytochrome *c* with cardiolipin-containing phospholipid vesicles, serving as models of the OMM, is investigated to probe cytochrome *c*-induced permeability. Lipid vesicles having either a 1,2-dipalmitoyl-*sn*-glycero-3-phosphocholine (DPPC) or mixed-DPPC/cardiolipin membrane and containing a membrane-impermeable Raman tracer 3-nitrobenzenesulfonate (3-NBS) were optically trapped, translated into a solution containing cytochrome *c*, and monitored for 3-NBS leakage. Cytochrome-correlated leakage was observed only in cardiolipin-containing vesicles. Structural changes observed in the Raman spectra during permeabilization indicated acyl chain disordering along with decreased intensity of the cardiolipin cis-double-bond stretching modes. When the vesicle-associated cytochrome *c* Raman spectrum is compared with a spectrum in buffer, heme-resonance bands are absent, indicating loss of Met-80 coordination. To verify selective interactions of cytochrome *c* with cardiolipin, these experiments were repeated where the DPPC acyl chains were deuterated (D62-DPPC), allowing spectral resolution of the DPPC acyl chain response from that of cardiolipin. Interestingly, D62-DPPC acyl chains were unaffected by cytochrome *c* accumulation, while cardiolipin showed major changes in acyl chain structure. These results suggest that cytochrome-induced permeabilization proceeds through selective interaction of cytochrome *c* with cardiolipin, resulting in protein unfolding, where the unfolded form interacts with cardiolipin acyl chains within the bilayer to induce permeability.

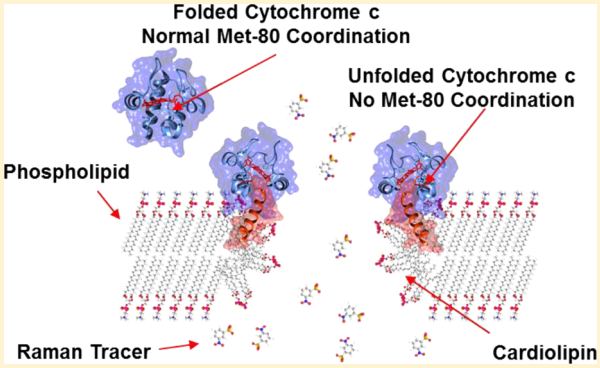

INTRODUCTION

Apoptosis, a genetically regulated form of cell death, is an essential function which controls cell proliferation and differentiation through programmed destruction of a cell following apoptotic activation via one of many intrinsic or extrinsic pathways.[1−3] Because abnormalities in the apoptotic pathway are associated with many disease states and disorders,[2,4,5] much scientific effort has been directed toward understanding apoptotic activation and the mechanism of apoptosis.[1] Through those research studies, it has been discovered that, although many activation pathways exist, the apoptotic process generally terminates in destruction of the cell via activation of the proteolytic series of caspase (cysteine-aspartic protease) proteins.[1,6] This activation is often preceded by the protein-induced permeabilization of the outer mitochondrial membrane,[1−3,7,8] which results in interruption of the cellular respiration process,[9,10] leads to ion and water permeability and mitochondrial swelling,[11,12] and causes a buildup of reactive oxygen species within the mitochondria through depletion of glutathione,[13] resulting in oxidative damage to mitochondrial proteins and lipids.[10,13−15] Eventually, pro-apoptotic signaling proteins are released, including Smac/DIABLO and Omi/HtrA2 (which activate caspase-3 and caspase-9 by blocking the action of inhibitor of apoptosis (IAP) proteins) and cytochrome *c*, which activates the caspase cascade through binding apoptotic protease activating factor 1 (APAF-1), leading to cleavage of procaspase-9 into the mature proteolytic form, caspase-9, proteins that remain localized within the mitochondria in healthy cells.[1,11] The importance of OMM permeabilization in apoptosis motivates research to understand how membrane permeabilization occurs, an important step in developing a complete picture of apoptosis.[16]

Despite considerable research effort, the steps resulting in induction of permeability remain poorly understood. One known mechanism of membrane permeation is the interaction of Bcl-2 proteins, bid, bak, and bax, which act as a cooperative complex to form pores in the OMM through which ions, water, and proteins can cross.[8,17,18] More recently, it has been proposed that cytochrome *c* not only acts as a signaling

Received: January 8, 2017
Published: February 21, 2017

DOI: 10.1021/jacs.7b00238
J. Am. Chem. Soc. 2017, 139, 3851−3860

molecule during apoptosis but actively participates in the permeabilization process.[16,19,20]

Cytochrome *c* is an electron-transport protein normally localized to the outer leaflet of the inner mitochondrial membrane (IMM) in healthy cells. Localization of cytochrome *c* to the IMM occurs through strong association with the divalent-anionic diphosphatidylglycerol lipid, cardiolipin, which comprises ~20 mol % of the IMM.[21−23] In early apoptotic cells, translocation of cardiolipin from the IMM to the outer mitochondrial membrane (OMM) leads to an outer-mitochondrial membrane comprising ~40 mol % cardiolipin.[21,22,24] Through buildup of reactive oxygen species in the intermembrane space, cytochrome *c*-catalyzed peroxidation of IMM-cardiolipin occurs, resulting in release of the strong cytochrome *c*−cardiolipin interaction, dissociating cytochrome *c* from the IMM and leading to translocation to the OMM;[21,25−28] here, it is hypothesized to participate in the permeabilization process.[19,28] Fluorescence spectroscopy experiments carried out in cardiolipin-containing (40 mol %) phospholipid vesicles, which act as a model of the OMM, have demonstrated cytochrome *c* induced membrane permeability which allowed large (10 kDa) dextran molecules and cytochrome *c* (12 kDa) itself to cross the membrane.[19] These results are compelling, and motivate further study of the cytochrome *c*−cardiolipin interaction which is hypothesized to drive the permeabilization process. While fluorescence experiments can provide insight into transport of molecules across the membrane, fluorescence spectroscopy provides little to no insight into the structure of cytochrome *c*, cardiolipin, or other membrane lipids as permeabilization occurs. In an attempt to understand and elucidate the lipid and cytochrome structures, nuclear magnetic resonance (NMR) and freeze-fracture transmission electron microscopy (TEM) techniques have been used *ex situ*, indicating partial unfolding of cytochrome *c* on interaction with cardiolipin and the formation of nonbilayer structures and atypical hexagonal lipid phases.[29,30] Additionally, Förster resonance energy transfer (FRET),[31] resonance Raman,[32,33] infrared absorbance,[34] and circular dichroism[31] experiments conducted *in situ* have provided insight into the cytochrome *c* structure upon interaction with cardiolipin with several mechanisms of unfolding and anchoring proposed, all indicating disruption of Met-80 coordination of the heme center and suggesting some degree of unfolding. Although these experiments provide valuable insight into the cardiolipin−cytochrome *c* interaction, they fail to provide simultaneous information on both permeability *and* chemical structure; thus, cytochrome *c*, cardiolipin, and lipid structures associated with permeabilization remain unknown. This information is essential to furthering the understanding of the interaction between cytochrome *c* and cardiolipin which results in permeabilization.

In this work, we meet these challenges by combining confocal Raman microscopy and optical trapping to monitor *simultaneously* the structure of cytochrome *c*, cardiolipin, and phospholipid in the membrane of individual vesicles that have been filled with a membrane-impermeable tracer molecule (3-nitrobenzenesulfonate, 3-NBS), which serves as a marker for membrane permeability. Raman microscopy has been previously combined with optical trapping to investigate phospholipid acyl chain structure in individual vesicles during the phospholipid phase transition,[35−37] to measure small-molecule contents of individual vesicles,[38,39] and to measure small-molecule association with vesicle membranes.[40] Additionally, Raman spectroscopy has been used previously to study the structure of cytochrome *c*[41,42] and to examine cytochrome *c* association with cardiolipin in a dispersion of pure cardiolipin liposomes.[33] Here, we investigate the interaction of cytochrome *c* with cardiolipin-containing phospholipid vesicles to probe the mechanism of cytochrome-induced permeability. DPPC (1,2-dipalmitoyl-*sn*-glycero-3-phosphocholine) vesicles were formed with and without cardiolipin (40 mol %) in a solution of a membrane-impermeable Raman tracer, 3-nitrobenzenesulfonate (3-NBS). Individual optically trapped vesicles were exposed to solutions of cytochrome *c* and monitored for 3-NBS leakage.

Optical trapping allows localization of an individual vesicle at a tight laser focus through the combination of a large electric field gradient produced by the tightly focused laser radiation and the difference in the dielectric contrast between the vesicle bilayer and the surrounding buffer solution.[43,44] If the optical-trapping force is great enough, a vesicle can be held in place while the stationary solution surrounding it is moved about;[38,39] this allows an individual optically trapped vesicle to be transferred into a buffer solution containing cytochrome *c*. By using the same laser radiation to perform optical trapping and to excite Raman scattering, the change in exterior-solution composition can be made while simultaneously collecting Raman scattered light, permitting simultaneous monitoring of cytochrome *c* accumulation, changes in the resonance Raman activity of cytochrome *c*, changes in DPPC acyl chain structure, and permeabilization of the membrane (reflected in the leakage of 3-NBS). The time-dependent spectra of membrane permeabilization are then analyzed using self-modeling curve resolution (SMCR), a multivariate statistical method which allows resolution of correlated spectral changes through eigenvector decomposition of the spectral data[45,46] (see the Supporting Information). SMCR analysis produces a set of "component" spectral vectors and corresponding composition vectors that describe the relative contribution of each component spectrum to the total observed spectrum (which comprises the composition-weighted sum of each component) at a given point in time. The resulting components and composition vectors provide insight into the chemical interactions and mechanism of membrane permeabilization.

MATERIALS AND METHODS

Reagents and Materials. Cytochrome *c* (equine, >95%), cardiolipin (bovine, >98%), and 3-nitrobenzenesulfonic acid sodium salt (98%) were obtained from Sigma-Aldrich and used without further purification. Cytochrome *c* purity was verified by SDS-PAGE (see the Supporting Information). Potassium phosphate monobasic, potassium chloride, and sodium phosphate dibasic (all >99%) were obtained from Fisher Scientific (Hampton, NH). Hydrochloric acid (36.5−38.0%), sodium chloride (99%), and sodium hydroxide (99%) were obtained from Avantor Performance Materials. DPPC (1,2-dipalmitoyl-*sn*-glycero-3-phosphocholine) and D62-DPPC (1,2-dipalmitoyl-d62-*sn*-glycero-3-phosphocholine) were obtained from Avanti Polar Lipids. Phospholipids were diluted into chloroform and stored at −20 °C until use.

Tracer (3-NBS) filled vesicles were formed by extrusion using the following procedure: aliquots of DPPC, D62-DPPC, and cardiolipin in chloroform were transferred to glass vials in ratios appropriate to produce either pure single-component vesicles or 40 mol % cardiolipin mixed vesicles. The samples were dried under a stream of nitrogen and placed under a vacuum (100 mTorr) for 1 h to ensure complete removal of the solvent. The lipid was then rehydrated in a warm (~60 °C, greater than the DPPC phase transition temperature) solution of 50 mM 3-NBS in phosphate buffered saline which was pH adjusted to pH 9.5, well above the 3-NBS pK_a of 6.7,[47] ensuring 3-NBS remained

DOI: 10.1021/jacs.7b00238
J. Am. Chem. Soc. 2017, 139, 3851−3860

in the charged, membrane-impermeable form[48] throughout experiments; the hydrated 1 mg/mL lipid dispersion was extruded through a polycarbonate track-etched membrane with 400 nm pores[49] using a Mini-Extruder (Avanti Polar Lipids) maintained at 60 °C to produce unilamellar vesicles of nominally 400 nm diameter.

A three-port microscopy cell for carrying out the manipulation of optically trapped vesicles was constructed and adapted for solution exchanging using Luer-lock fittings and Viton elastomer tubing. A diagram of the cell and detailed description are presented in the Supporting Information. A diagram and description of the microscopy well-cell used for measuring concentrated solution-phase cytochrome *c* samples has been published previously.[50]

Optical-Trapping Confocal Raman Microscopy. A detailed description of the confocal Raman microscope used in this work has been published previously.[50,51] In brief, the beam from a Kr^+ laser (Coherent Inc.) is passed through a bandpass filter (Semrock), beam expanded (Special Optics Inc.), directed into an inverted fluorescence microscope frame (Nikon), and reflected off of a dichroic mirror (Semrock) to slightly overfill the back aperture of a 100×, 1.4 numerical-aperture microscope objective. Laser radiation is focused by the objective to an ~600 nm diameter spot where, through the combination of a large intensity gradient and the dielectric contrast between phospholipid and water, an individual vesicle can be optically trapped[43,44] and translated about in solution.[38,39] Scattered radiation is collected back through the objective, passed through the same dichroic mirror, collimated, passed through a holographic notch filter (Kaiser Optical Systems), and focused onto the monochromator entrance slit. The Raman scattered light is dispersed by a diffraction grating and focused onto a CCD camera. The confocal aperture is defined in the vertical dimension by the monochromator entrance slit (50 μm) and in the horizontal dimension by binning three rows on the CCD camera (78 μm),[52] producing an ~1 fL confocal probe volume.

For experiments where an individual vesicle is manipulated from buffer solution into cytochrome *c* solution, the three-port microscopy cell is flushed with buffer and then filled with vesicle suspension (Figure S-2A and S-2B). The first inlet port is blocked, and a solution of the same buffer containing cytochrome *c* is introduced at the midpoint inlet and allowed to fill the channel between the midpoint and the outlet (Figure S-2C). The microscope stage is then translated in the *x*, *y*, and *z* dimensions to localize the laser focus near a vesicle in the vesicle suspension between the first and middle inlets; the large intensity gradient produced by the focused laser radiation attracts the vesicle into the laser focus where it remains trapped (confirmed by observing through the microscope eyepiece). The microscope stage is then translated in the *x* and *y* dimensions to manipulate the microscopy cell, bringing the vesicle through the channel and into the cytochrome *c* solution between the midpoint inlet and outlet (Figure S-2D). Raman scattering is measured throughout with sequential 10 s integration times. The time axis is initiated (t = 0) at the point where the vesicle has crossed the solution boundaries confirmed visually by the vesicle passing under the midpoint inlet. All vesicles were brought to the far end of the flow channel (away from the vesicle suspension/cytochrome *c* solution boundary) to ensure mixing did not alter the cytochrome *c* concentration surrounding the vesicle. Experiments were carried out at room temperature (~21 °C).

Spectral Processing and Data Analysis. All Raman spectra were baseline corrected using custom Matlab scripts. Matlab was also used for self-modeling curve resolution (SMCR)[45] analysis of the time-dependent cytochrome *c*-induced permeabilization experiments. Details of the spectral correction and SMCR analyses are presented in the Supporting Information.

RESULTS AND DISCUSSION

Structure of Cytochrome *c*, Cardiolipin, and DPPC during Permeabilization of Cardiolipin-Containing Lipid Membranes. To investigate the mechanism of cytochrome *c*-induced permeabilization of cardiolipin-containing phospholipid membranes, cytochrome *c*, cardiolipin, and phospholipid were simultaneously monitored using Raman spectroscopy. Individual, 3-NBS tracer-filled phospholipid vesicles were optically trapped and moved from a buffer solution into a solution of 100 μM cytochrome *c*. Once in cytochrome *c* solution, Raman scattering from the vesicle and tracer was monitored as a function of time (Figure 1).

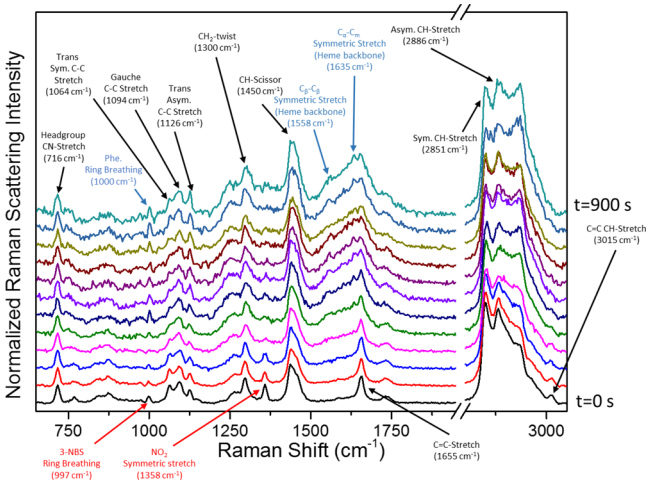

Figure 1. Raman spectra of an individual, optically trapped, 3-NBS filled cardiolipin-containing (40 mol % cardiolipin in DPPC) vesicle collected as a function of time during exposure to 100 μM cytochrome *c*. The initial time, t = 0, is when the vesicle was first manipulated into the cytochrome *c* solution. Phospholipid vibrational modes are labeled in black, cytochrome *c* Raman modes in blue, and 3-NBS Raman modes in red.

Cytochrome *c* induced membrane permeabilization (observed through disappearance of the 3-NBS NO_2-symmetric stretching mode (1358 cm^{-1}) and ring breathing mode (997 cm^{-1})),[48] along with cytochrome *c* accumulation (observed through the increases in Raman modes in the amide I stretching (1550−1700 cm^{-1}) and peptide backbone carbon−hydrogen (C−H) stretching (2935 cm^{-1}) regions of the spectrum),[53] was observed in DPPC + 40 mol % cardiolipin vesicles (Figure 1). Neither membrane permeability nor protein accumulation was observed in pure DPPC vesicles, or in experiments where cytochrome *c* was first thermally denatured, even after periods of 1000 s, far exceeding the (~300 s) time required for complete leakage of 3-NBS from cardiolipin-containing vesicles of the same size (see the Supporting Information).

To elucidate structure changes from the spectra associated with membrane permeabilization, we employ self-modeling curve resolution (SMCR), a multivariate statistical method which allows resolution of correlated spectral changes through eigenvector decomposition of the spectral data (see the Supporting Information).[45,46] The factor analysis step in SMCR[46] indicates that two significant components are responsible for 99.7% of the variance in the time-dependent spectra; rotation of the eigenvector representations of this variation into the real space of the component spectra and their time dependence provides insight into the process. The two component responses observed in the spectra during membrane permeabilization (Figure 2A) and how those changes evolve as a function of time (Figure 2B) are associated with (1) cytochrome accumulation and 3-NBS leakage (red) and (2) intact cardiolipin-containing vesicles filled with 3-NBS (black). To more readily compare these spectra, a difference

DOI: 10.1021/jacs.7b00238
J. Am. Chem. Soc. 2017, 139, 3851−3860

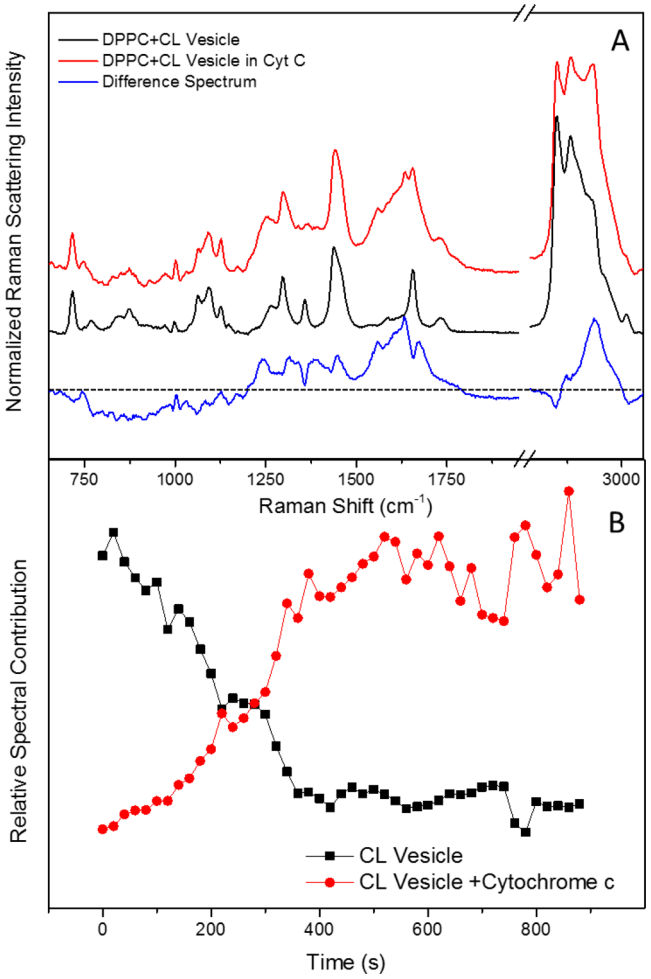

Figure 2. Results of SMCR analysis of cytochrome *c*-induced permeability of cardiolipin-containing (40 mol % cardiolipin in DPPC) vesicles. (A) Component Raman spectra obtained from SMCR analysis corresponding to the nonpermeable cardiolipin-containing DPPC vesicle (black), the cytochrome *c* exposed, permeable, vesicle (red), and a difference spectrum (blue). (B) The relative contribution of the two components in part A to the overall spectra as a function of time.

spectrum (blue) is also presented in Figure 3. In the following discussion, the structure changes associated with membrane permeability will be discussed in terms of the chemical species involved.

Cytochrome c. In the cytochrome *c* specific regions of the Raman spectrum, a number of changes are observed. Beginning with the low-frequency region, the most notable change observed concurrent with 3-NBS leakage is the appearance of the phenylalanine ring breathing mode at 1000 cm^{-1} which indicates the appearance of protein. At higher frequency, the appearance and continued increase of modes near the amide I region of the Raman spectrum (1550−1700 cm^{-1}) are observed. The peaks in this region of the spectrum are highly overlapping, making analysis of specific structures challenging, especially with the signal-to-noise limits imposed by fast acquisition times (10 s) required for time-dependent experiments. By extracting the correlated changes across the entire data set, SMCR provides a better picture of the region than is observed in individual spectra (Figure 2A). Careful analysis of this region, then, provides insight into the structure of the vesicle-associated protein. The first prominent feature observed

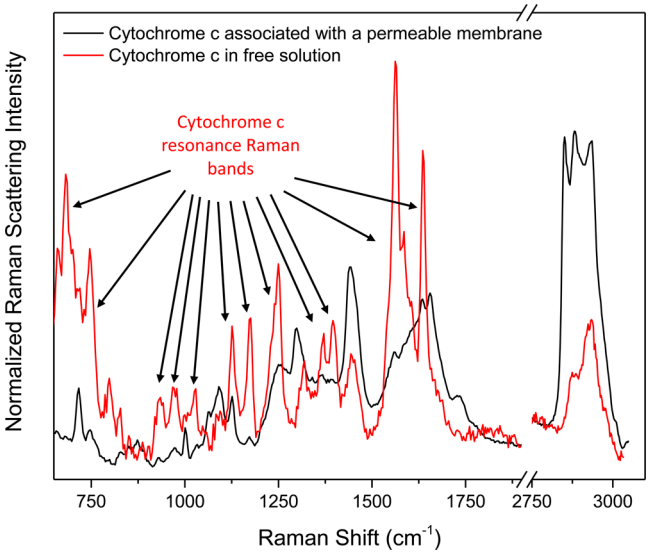

Figure 3. Comparison of the resonance-enhanced free-solution spectrum of cytochrome *c* (red) to cardiolipin containing vesicle (40 mol % cardiolipin in DPPC) associated cytochrome *c* (black) where the resonance Raman modes have disappeared due to disruption of Met 80−Heme coordination.

at 1558 cm^{-1} has been previously assigned to the C_β−C_β (using the labeling scheme of ref 41) symmetric stretching from the pair of carbon atoms opposite the nitrogen in the pyrrole subunits of the cytochrome *c* heme center,[41] indicating the adsorbed protein is indeed cytochrome *c*. The next most prominent feature is a broad peak at 1611 cm^{-1} which appears as a shoulder on the band at 1631 cm^{-1}. The broad 1611 cm^{-1} band has been assigned to Trp, Tyr, and Phe side chain vibrations when incorporated in α-helical structures;[53] normally occurring at higher (1620 cm^{-1}) frequency, this mode is shifted to lower frequency in proteins with interspersed α-helical and β-sheet secondary structures, suggesting a mixed tertiary structure in the cardiolipin-bound cytochrome *c*.[53] This is supported by the presence of the strong amide I band at 1674 cm^{-1} (more easily visualized in the difference spectrum) which in purely α-helical proteins occurs closer to 1655 cm^{-1} but is observed at higher frequency in both purely β-sheet and mixed α-helix and β-sheet proteins,[53,54] and β-turn structures.[55] Although β-turns are anticipated on the basis of the native structure of cytochrome *c*, mixed α-helix and β-sheet structures are not;[56] thus, observation of these modes was unexpected in this work. However, previous UV resonance Raman work has shown that at high temperature cytochrome *c* adopts an unfolded conformation wherein formation of β-sheet structure occurs along the 40s Ω loop along with loss of Met 80 coordination of the heme.[56] It has been proposed on the basis of deuterium exchange,[30] circular dichroism,[31,57] Fourier transform infrared,[33,34] fluorescence,[31,57] and previous Raman spectroscopy[33] work that similar unfolding occurs on association of cytochrome *c* with cardiolipin; the presence of these mixed secondary structure Raman bands supports the conclusion of protein unfolding and provides further evidence of β-sheet structure in the unfolded state. At a slightly higher frequency than the 1611 cm^{-1} band is an additional heme vibration (1631 cm^{-1}) which has been assigned to ν10 (C_α−C_m of the backbone linkage between the pyrrole rings in the heme center).[41]

DOI: 10.1021/jacs.7b00238
J. Am. Chem. Soc. 2017, 139, 3851−3860

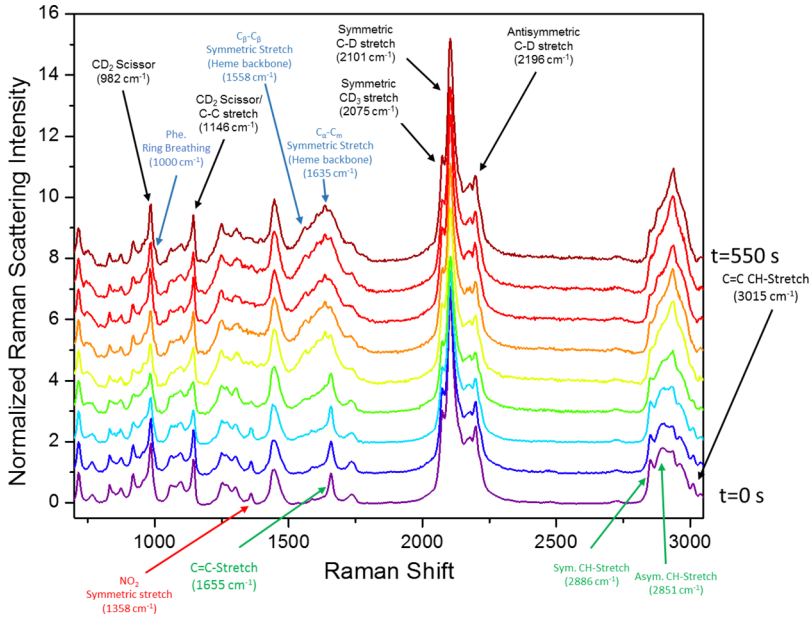

Figure 4. Raman spectra of an individual, optically trapped, 3-NBS filled, cardiolipin-containing (40 mol % cardiolipin in D62-DPPC) vesicle, where the DPPC acyl chains have been deuterated to allow spectral resolution of DPPC vibrational modes from cardiolipin vibrational modes. The spectra were collected as a function of time during exposure to 100 μM cytochrome *c*. Initial time, $t = 0$, is when the vesicle was first manipulated into the cytochrome *c* solution. DPPC Raman modes are highlighted in black, cardiolipin Raman modes in green, cytochrome *c* Raman modes in blue, and 3-NBS Raman modes in red.

The cytochrome *c* spectrum presented in Figure 2 is interesting when compared with a spectrum of free solution cytochrome *c* (Figure 3) excited using the same $\lambda = 647$ nm source. In the free solution case, a number of intense bands are present that are either absent or of weak intensity in the cardiolipin-associated cytochrome *c* spectrum. The Raman bands in the free-solution case are in good agreement with previous resonance Raman investigations, where the excitation was within the Met 80−heme charge-transfer excitation band centered at $\lambda = 695$ nm. This indicates that the 647 nm excitation used in the current work lies within the Met 80 charge transfer band, leading to resonance enhancement of the Raman scattering from the heme center of cytochrome *c* in free solution.[58,59]

The reduction in intensity and disappearance of resonance Raman vibrational modes in the spectrum of cardiolipin-associated cytochrome *c* suggests a structural change in the protein upon association with cardiolipin that leads to the loss of Met 80 coordination, eliminating the charge-transfer band and thereby the resonance Raman modes observed in the free solution spectrum. To test this, the electronic absorption spectrum of cytochrome *c* in buffer was compared with the spectrum of cytochrome *c* in a solution of excess cardiolipin vesicles (see the Supporting Information) where the 695 nm charge-transfer band is clearly absent in the cardiolipin-associated case; this provides further evidence of cytochrome *c* unfolding upon interaction with cardiolipin. This result, combined with the structural insights gained from the nonresonance Raman bands, suggests that cytochrome *c* unfolds upon interaction with cardiolipin, which is correlated with permeabilization of the cardiolipin-containing membrane.

Cardiolipin and DPPC. Raman scattering from the cardiolipin and DPPC acyl chains provides insight into the impact of cytochrome *c* association on the phospholipid membrane structure. In the C−C stretching region of the spectrum (1030−1150 cm^{-1}), the ratio of the intensity of the C−C antisymmetric stretching mode (1062 cm^{-1}) to the C−C gauche conformer stretching (1086 cm^{-1}) is indicative of acyl chain ordering, where a decrease in I_{1062}/I_{1086} intensity ratio suggests the bilayer contains more gauche conformers and is less ordered.[60] As cytochrome *c* accumulates and the membrane becomes permeable, I_{1062}/I_{1086} changes from 0.85 ± 0.06 to 0.64 ± 0.06, indicating that acyl chain ordering is disrupted by cytochrome *c* association. Additional evidence of acyl chain disordering is observed in the C−H twisting region of the spectrum where the CH_2 twisting mode (1295 cm^{-1}) decreases in intensity, broadens, and shifts to higher frequency due to increased rotational and vibrational freedom of hydrogen atoms about the carbon backbone.[36,37,54,60,61] In the C−H bending region of the spectrum, overlap of C−H bending from the protein backbone structure makes interpretation of the spectrum challenging. However, by comparing the difference spectrum with the component spectra, a qualitative picture of changes in acyl chain lattice order can be gained. A decrease in acyl chain lattice order is typically observed in a decrease in the ratio of the antisymmetric methyl bend (1436 cm^{-1}) to the methylene scissoring mode (1455 cm^{-1});[60] in the difference spectrum in Figure 2, an overlapping peak at 1443 cm^{-1} appears due to cytochrome *c* backbone C−H bending. Despite the amplitude this mode adds to the antisymmetric stretching mode, the ratio I_{1436}/I_{1455} is still decreased (1.25 to 1.11), indicating a loss of lattice ordering in the bilayer acyl chains. Similarly, in the C−H stretching region of the spectrum, the ratio of the antisymmetric C−H stretching mode (2883 cm^{-1}) to the symmetric C−H stretching mode (2847 cm^{-1}) indicates acyl chain lateral packing density.[36,37,54,60,61] When the packing density is high, as in the case of ordered acyl chains, dipolar coupling between methylene C−H vibrations in adjacent chains leads to an increase in the intensity of the CH_2 symmetric stretching mode and a decrease in I_{2883}/I_{2847}. In these spectra, the protein backbone C−H stretching modes overlap the antisymmetric stretching mode (2883 cm^{-1}) of the phospho-

DOI: 10.1021/jacs.7b00238
J. Am. Chem. Soc. 2017, 139, 3851−3860

lipid acyl chains, causing the ratio of these peaks to be a poor indicator of bilayer structure. In the difference spectrum, however, a decrease in the C−H symmetric stretching mode *is* observed, indicating a decrease in acyl chain methylene C−H vibrational coupling that arises from disordered acyl chains.

Perhaps the most compelling observation in the spectrum of the cytochrome *c* associated membrane lies in the C═C modes[33,62] where a decrease is observed in the intensity of the C═C stretching mode (1655 cm^{-1}) and the C—H stretching mode of the cis-double bond associated ═C—H stretching mode (3011 cm^{-1}). Because the DPPC is fully saturated, the C═C related scattering arises entirely from the cardiolipin double bonds, where the intensity changes in these modes indicate a cytochrome *c*-specific interaction with cardiolipin; additionally, the position of the C═C double bonds (positions 9 and 12 on the cardiolipin acyl chains) suggests that cytochrome *c* alters the acyl chain environment deep within the cardiolipin acyl chains.[33] These results are in agreement with recent work where circular dichroism and FRET measurements of cytochrome *c* associated with cardiolipin-containing bilayers indicated that the protein adopts an unfolded conformation on interaction with cardiolipin and also that the unfolded α-helix is located in a hydrophobic environment (based on blue shifting of the fluorescence spectrum of the labeled helix).[31] Additionally, cardiolipin-specific changes in the membrane structure are consistent with previous literature where cytochrome *c* has been shown to induce nonlamellar polymorphic structures including inverted hexagonal (H_{II}) phases (cylindrical, headgroup-lined aqueous phases) in cardiolipin-containing bilayers.[29]

These results provide insight into the structure of cytochrome *c* and the cardiolipin-containing bilayer upon mutual association. However, observing cytochrome *c*-induced permeabilization only in cardiolipin-containing membranes and the intensity changes in the cardiolipin-specific C═C stretching modes, while also finding intensity changes in C—C and C—H stretching modes associated with *both* cardiolipin and DPPC acyl chains, raises questions regarding the nature of the permeable membrane: Where does permeabilization occur? Is it through long-range disordering of the entire bilayer, or is the disordering localized to cardiolipin?

Cytochrome *c* Association with a Membrane Containing Isotopically Labeled DPPC. To investigate the specificity of cytochrome *c*-induced permeabilization of cardiolipin-containing membranes, an experiment was carried out where the DPPC acyl chains were deuterated (1,2-dipalmitoyl-d62-*sn*-glycero-3-phosphocholine, D62-DPPC), allowing spectral resolution of the DPPC acyl chain Raman bands from the cardiolipin bands (Figure 4). SMCR analysis of 3-NBS leakage from these vesicles identified two component spectra, one corresponding to the initial bilayer without cytochrome *c* association and the other a cytochrome *c*-associated permeable bilayer (Figure 5). Membrane permeability is again indicated by the disappearance of the 3-NBS NO_2-symmetric stretching (1358 cm^{-1}) and ring breathing (997 cm^{-1}) modes, and cytochrome *c* accumulation through the increases in Raman modes in the amide I stretching (1550−1700 cm^{-1}) and peptide backbone carbon−hydrogen (C−H) stretching (2935 cm^{-1}) regions of the spectrum. The species-specific changes in the Raman spectra are presented below.

Cytochrome c. In the cytochrome *c* specific regions of the Raman spectrum, similar changes are observed compared to the nondeuterated case. In the difference spectrum, we again see the appearance of the phenylalanine ring breathing mode at 1000 cm^{-1}. The modes near the amide I region of the Raman spectrum including the C_β−C_β stretch (1558 cm^{-1}), the broad peak at 1611 cm^{-1} corresponding to Trp, Tyr, and Phe ring vibrations, the strong amide I band at 1674 cm^{-1}, and the C_α−C_m stretching mode (1631 cm^{-1}) appear at the same frequency in both deuterated and nondeuterated cases, indicating cytochrome *c* structure on association is unaffected by deuteration of the DPPC acyl chains.

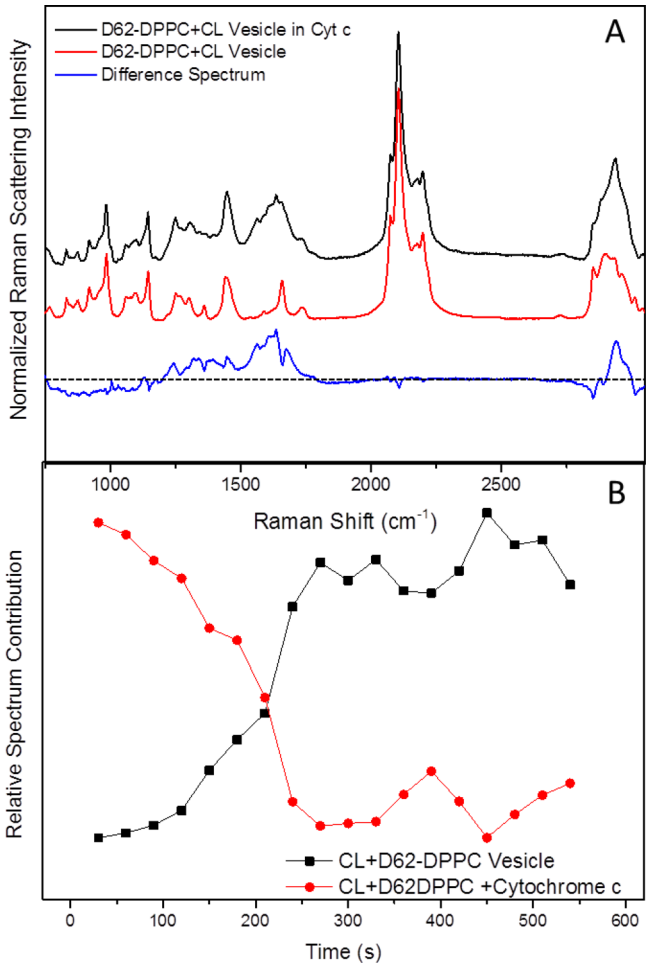

Figure 5. Results of SMCR analysis of cytochrome *c*-induced permeability of cardiolipin-DPPCD62 (40 mol % cardiolipin) vesicles. (A) Component Raman spectra obtained from SMCR analysis corresponding to the nonpermeable cardiolipin-containing DPPC-D54 vesicle (black), the cytochrome *c* exposed, permeable, vesicle (red), and a difference spectrum (blue). (B) The relative contribution of each component in part A to the overall spectrum as a function of time.

Cardiolipin. By using DPPC with deuterated acyl chains (D62-DPPC), it was possible to resolve Raman scattering of the cardiolipin acyl chain structure from that of DPPC during permabilization. In the cardiolipin specific (C−C(H) and C−H acyl chain vibrational modes) regions of the spectrum, similar changes are observed in both the deuterated and nondeuterated DPPC experiments. The ratio of the intensity of the C−C antisymmetric stretching mode (1062 cm^{-1}) to the C−C gauche conformer stretching (1086 cm^{-1}) I_{1062}/I_{1086} changes from 0.82 ± 0.02 to 0.76 ± 0.02, in this case indicating *specifically* that cardiolipin acyl chain ordering is disrupted by cytochrome *c* association during permeabilization. Due to the

DOI: 10.1021/jacs.7b00238
J. Am. Chem. Soc. 2017, 139, 3851−3860

loss of Raman scattering intensity from protonated acyl chains (due to the ~80% decrease in protonated acyl chains of DPPC), interpretation of the CH_2 twisting (1295 cm^{-1}) and CH bending (1430−1460 cm^{-1}) is challenging, because Raman scattering from cytochrome *c* begins to overlap these regions. Qualitatively, a decrease in acyl chain lattice order is indicated by broadening of the CH_2 twisting mode. In the C−H bending region, I_{1436}/I_{1455} remains the same despite the appearance of an overlapping peak at 1443 cm^{-1} from the cytochrome *c* backbone C−H bending (which should increase the ratio), indicating the ratio is decreased, and a change in cardiolipin acyl chain packing density in the permeable membrane. In the C−H stretching region of the spectrum, the protein backbone modes are overlapped; nevertheless, a decrease in intensity of the symmetric C−H stretching mode suggests that the ratio of the antisymmetric C−H stretching mode (2883 cm^{-1}) to the symmetric C−H stretching mode (2847 cm^{-1}) is decreased and that C−H dipolar coupling between adjacent cardiolipin acyl chains is disrupted.

In the C═C stretching regions of the cardiolipin spectrum, the intensity of the C═C double bond stretching mode (1655 cm^{-1}) and the C—H stretching mode of the cis-double bond associated ═C—H stretching mode (3011 cm^{-1}) decrease similarly to the nondeuterated case, again indicating a cytochrome *c* specific interaction with cardiolipin which alters the environment local to the double bonds deep within the membrane.[33] In agreement with previous work,[31,56] the results are consistent with the protein adopting an unfolded conformation upon interaction with cardiolipin where the unfolded protein adopts a β-sheet structure, and the terminal α-helix is located in a hydrophobic environment.

DPPC. Interestingly, no changes are observed in the C−C(D) stretching (symmetric, 830 cm^{-1}; antisymmetric, 1140 cm^{-1}), CD_2 twisting (916 cm^{-1}), CD scissoring (981 cm^{-1}), or CD stretching (2000−2250 cm^{-1}) modes from the DPPC acyl chains. This indicates that, despite extensive interaction of cytochrome *c* with cardiolipin, this interaction has *no impact* on the acyl chain structure of the surrounding DPPC lipids which remain well-ordered and dominated by trans conformers. The results suggest that membrane permeability occurs *exclusively* through association of cytochrome *c* with cardiolipin, resulting in distinct changes in both cardiolipin and cytochrome *c* structure (Figure 5) but no changes in DPPC. The lack of any detectable impact on the chain conformations of the DPPC acyl chains suggests that cardiolipin and DPPC are segregated when cytochrome *c* associates with the membrane.

It has been shown previously that certain proteins preferentially associate with unsaturated acyl chains.[63,64] Thus, we carried out an experiment to test whether the selective interaction of cytochrome *c* with cardiolipin might arise simply from a stronger interaction with unsaturated acyl chains of the cardiolipin compared to the saturated DPPC lipid in which it was dissolved. Vesicles having membranes of an unsaturated lipid, 1-palmitoyl-2-oleoylphosphatidylcholine (POPC), were optically trapped, manipulated into a solution of cytochrome *c*, and monitored for cytochrome *c* accumulation (see the Supporting Information). In these experiments, no cytochrome *c* accumulation could be detected over a time period exceeding the time required for cytochrome accumulation and 3-NBS leakage in cardiolipin-containing DPPC vesicles, which confirms the selective association of cytochrome *c* with cardiolipin.

Investigating the Nature of the Cytochrome *c* Induced Membrane Permeability. Although cytochrome *c*-induced permeabilization of cardiolipin-containing membranes to 3-NBS occurs in both deuterated and nondeuterated DPPC experiments, this result does not provide evidence of the nature of the defects in the membrane that allow the tracer to escape. Permeabilization of membranes is known to occur through phase boundaries in lipids near their phase transition temperature, and similar boundaries could be introduced by the presence of cytochrome *c* in the membrane.[65]

It has been previously shown that the NO_2-symmetric stretching mode of 3-NBS is sensitive to its surroundings, where the peak shifts to lower frequency and decreases in intensity in a hydrophobic environment compared to water. This property has been used previously[48] to characterize the nature of pores formed in vesicle membranes, to determine whether 3-NBS leakage at the phase transition occurs through partitioning (shifting of the NO_2-symmetric stretching mode followed by 3-NBS disappearance) or through water-filled pores (no-shift in the NO_2-symmetric stretching mode) in vesicles stabilized by the presence of lysolipid and poly(ethylene glycol)-modified lipids in the membrane.

To gain a better understanding of the nature of the pores formed in cytochrome *c* permeabilized cardiolipin-containing membranes, therefore, we examine the NO_2-symmetric stretching mode during 3-NBS leakage (see Figure S-6, Supporting Information). No shift in the NO_2-symmetric stretching mode can be detected, indicating that no significant population of 3-NBS partitions into the hydrophobic lipid acyl chains during permeabilization, and therefore escape from the vesicle likely occurs through pores in the membrane. This result agrees with earlier literature where cytochrome *c*-induced permeability permits much larger macromolecules (10 kDa dextran and 12 kDa cytochrome *c*)[31] to cross the membrane which are unlikely to cross via partitioning into the acyl chains. In these experiments, as well as in the previous literature,[16,19] long times are required for complete equilibration of interior and exterior solutions. The time scale of the 3-NBS leakage (hundreds of seconds) is more than 6 orders of magnitude slower than anticipated for free-solution diffusion from a 200 nm radius sphere,[66] indicating that transport is significantly hindered. This result suggests a transient-pore mechanism where a small number of pores are open for a limited time, hindering escape of 3-NBS from the vesicle. This hypothesis is in agreement with previous reports in the literature,[16] which have shown that pore formation in cardiolipin-containing membranes is cytochrome *c*-concentration-dependent. When combined with the cardiolipin specificity of cytochrome *c*-induced permeabilization, a mechanism of pore formation is suggested, where cardiolipin-associated cytochrome *c* molecules may diffuse on the membrane until a sufficient number come within close proximity to form a transient pore. This pore formation mechanism is in agreement with ion-conductance measurements of cytochrome *c*-induced pores in planar lipid bilayers at an electrode interface, where transient pore formation was observed through intermittent current transients across cytochrome *c*-exposed cardiolipin membranes.[67]

Conclusions. Permeabilization of the outer mitochondrial membrane is a key step in apoptosis; translocation of cardiolipin, followed by cytochrome *c*, from the inner to the outer mitochondrial membrane appears integral to this process, and it has been suggested that the presence of cytochrome *c* in the outer mitochondrial membrane may contribute to

DOI: 10.1021/jacs.7b00238
J. Am. Chem. Soc. 2017, 139, 3851−3860

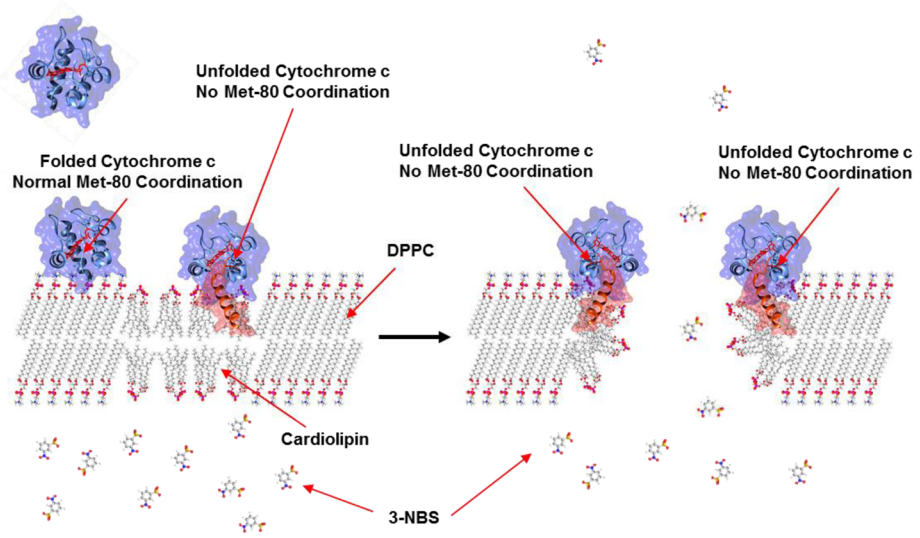

Figure 6. Proposed mechanism for cytochrome *c* induced membrane permeabilization based on Raman spectroscopic evidence.

membrane permeabilization. In this paper, we have applied an *in situ* spectroscopic method to evaluate the mechanism of outer mitochondrial membrane permeabilization, where phospholipid vesicles formed from mixed cardiolipin–DPPC bilayers were used as models of the apoptotic outer mitochondrial membrane. By forming vesicles in a solution of a membrane-impermeable tracer (3-NBS), it was possible to monitor membrane permeability with optical-trapping confocal Raman microscopy as vesicles were exposed to a solution of cytochrome *c*, thereby allowing investigation of the mechanism of cytochrome-induced permeabilization. Cytochrome *c*-induced 3-NBS leakage was observed only in cardiolipin-containing membranes, and permeabilization was not induced by thermally denatured cytochrome *c*. Structural changes observed in the Raman spectra during cytochrome *c* interaction with cardiolipin-containing vesicles, as 3-NBS was released, indicate that membrane permeabilization is associated with a loss of acyl chain ordering along with decreases in prominent carbon–carbon double bond stretching modes from the cardiolipin acyl chains. When the cardiolipin-vesicle-associated cytochrome *c* spectrum is compared with a solution-phase spectrum, prominent bands associated with heme resonance Raman are absent, indicating loss of Met 80 coordination of the heme, which suggests a structural change to the protein. These results suggest a mechanism for cytochrome *c*-induced permeabilization where the c-terminal α-helix of cytochrome *c* unfolds upon interaction with the cardiolipin-containing membrane (resulting in loss of heme coordination) and the unfolded helix associates with the cardiolipin acyl chains deep (nine carbons, ~1.4 nm) within the bilayer, as illustrated in Figure 6.

To understand the impact of the cytochrome–cardiolipin interaction on the membrane structure, the same experiments were carried out in vesicles where the DPPC acyl chains were deuterated (D62-DPPC), allowing spectral resolution of the phospholipid acyl chain structure from that of cardiolipin. Interestingly, the acyl chain order of D62-DPPC remained unaffected by cytochrome *c*, as indicated by lack of changes in the deuterated acyl chain vibrational modes, while the cardiolipin structure showed major changes indicated by the protonated acyl chain carbon–carbon and carbon–hydrogen stretching modes of the Raman spectrum; these results indicate that cytochrome *c*-induced permeability likely arises from unfolded cytochrome interacting *specifically* with cardiolipin and that cardiolipin appears to be segregated from the DPPC in the membrane.

The nature of membrane permeabilization was investigated by examining the environment-sensitive NO_2 symmetric stretching mode from 3-NBS during vesicle permeabilization. Lack of shifting in this mode during permeabilization suggests that 3-NBS escapes from the vesicle through pores, in agreement with cytochrome *c*-induced permeability of much larger molecules demonstrated in previous work. The escape of 3-NBS is significantly hindered compared with free-solution diffusion, suggesting that the membrane is not an open-pore network but is likely perforated with a small population of transient pores that form through the interaction of cardiolipin-associated cytochrome *c* molecules.

Confocal Raman microscopy has provided new mechanistic understanding of the role of cytochrome *c* in outer mitochondrial membrane permeabilization, a key step in the early stages of apoptosis. Further understanding of the apoptotic mechanism is important for developing a picture of the steps of cell differentiation and is essential to furthering our understanding of various disease states, including cancer, developmental disorders, and autoimmune diseases, in which dysfunction of apoptosis is implicated as a major contributor to the disease state.[2,4,5]

■ ASSOCIATED CONTENT

Supporting Information

The Supporting Information is available free of charge on the ACS Publications website at DOI: 10.1021/jacs.7b00238.

Additional information on verification of cytochrome *c* purity, description of the flow cell and self-modeling curve resolution analysis; cardiolipin-free, unsaturated-lipid, and denatured-cytochrome *c* control experiments, and UV–vis absorption spectra of the methionine-80 charge-transfer band (PDF)

■ AUTHOR INFORMATION

Corresponding Author

*harrisj@chem.utah.edu

DOI: 10.1021/jacs.7b00238
J. Am. Chem. Soc. 2017, 139, 3851–3860

ORCID
Shelley D. Minteer: 0000-0002-5788-2249
Joel M. Harris: 0000-0002-7081-8188

Notes

The authors declare no competing financial interest.

■ ACKNOWLEDGMENTS

This research was supported in part with funds from the U.S. Department of Energy (DE-FG03-93ER14333) to J.M.H. and by a grant from the Air Force Office of Scientific Research (FA9550-16-1-0279) to S.D.M. The assistance of Ross Milton in acquiring SDS-PAGE results for the cytochrome *c* sample is gratefully acknowledged.

■ REFERENCES

(1) Elmore, S. *Toxicol. Pathol.* **2007**, *35*, 495−516.
(2) Merry, D. E.; Korsmeyer, S. J. *Annu. Rev. Neurosci.* **1997**, *20*, 245−267.
(3) Adams, J. M.; Cory, S. *Science* **1998**, *281*, 1322−1326.
(4) Favaloro, B.; Allocati, N.; Graziano, V.; Di Ilio, C.; De Laurenzi, V. *Aging* **2012**, *4*, 330−349.
(5) Honig, L. S.; Rosenberg, R. N. *Am. J. Med.* **2000**, *108*, 317−330.
(6) McIlwain, D. R.; Berger, T.; Mak, T. W. *Cold Spring Harbor Perspect. Biol.* **2013**, *5*, a008656.
(7) Tsujimoto, Y. *Genes Cells* **1998**, *3*, 697−707.
(8) Jürgensmeier, J. M.; Xie, Z.; Deveraux, Q.; Ellerby, L.; Bredesen, D.; Reed, J. C. *Proc. Natl. Acad. Sci. U. S. A.* **1998**, *95*, 4997−5002.
(9) Harris, M.; Thompson, C. *Cell Death Differ.* **2000**, *7*, 1182.
(10) Ribas, V.; García-Ruiz, C.; Fernández-Checa, J. C. *Front. Pharmacol.* **2014**, *5*, 151.
(11) Desagher, S.; Martinou, J.-C. *Trends Cell Biol.* **2000**, *10*, 369−377.
(12) Snart, R. S. *Biochim. Biophys. Acta, Lipids Lipid Metab.* **1967**, *144*, 10−17.
(13) Armstrong, J. S.; Jones, D. P. *FASEB J.* **2002**, *16*, 1263−1265.
(14) Marí, M.; Morales, A.; Colell, A.; García-Ruiz, C.; Fernández-Checa, J. C. *Antioxid. Redox Signaling* **2009**, *11*, 2685−2700.
(15) Murphy, M. P. *Biochem. J.* **2009**, *417*, 1−13.
(16) Xu, J.; Vanderlick, T. K.; Beales, P. A. *PLoS One* **2013**, *8*, e69492.
(17) Korsmeyer, S.; Wei, M.; Saito, M.t.; Weiler, S.; Oh, K.; Schlesinger, P. *Cell Death Differ.* **2000**, *7*, 1166−1173.
(18) Wei, M. C.; Zong, W.-X.; Cheng, E.H.-Y.; Lindsten, T.; Panoutsakopoulou, V.; Ross, A. J.; Roth, K. A.; MacGregor, G. R.; Thompson, C. B.; Korsmeyer, S. J. *Science* **2001**, *292*, 727−730.
(19) Bergstrom, C. L.; Beales, P. A.; Lv, Y.; Vanderlick, T. K.; Groves, J. T. *Proc. Natl. Acad. Sci. U. S. A.* **2013**, *110*, 6269−6274.
(20) Firsov, A. M.; Kotova, E. A.; Korepanova, E. A.; Osipov, A. N.; Antonenko, Y. N. *Biochim. Biophys. Acta, Biomembr.* **2015**, *1848*, 767−774.
(21) Orrenius, S.; Zhivotovsky, B. *Nat. Chem. Biol.* **2005**, *1*, 188−189.
(22) Schug, Z. T.; Gottlieb, E. *Biochim. Biophys. Acta, Biomembr.* **2009**, *1788*, 2022−2031.
(23) Iverson, S. L.; Orrenius, S. *Arch. Biochem. Biophys.* **2004**, *423*, 37−46.
(24) Fernandez, M. G.; Troiano, L.; Moretti, L.; Nasi, M.; Pinti, M.; Salvioli, S.; Dobrucki, J.; Cossarizza, A. *Cell Growth Differ.* **2002**, *13*, 449−455.
(25) Shidoji, Y.; Hayashi, K.; Komura, S.; Ohishi, N.; Yagi, K. *Biochem. Biophys. Res. Commun.* **1999**, *264*, 343−347.
(26) Kagan, V. E.; Tyurin, V. A.; Jiang, J.; Tyurina, Y. Y.; Ritov, V. B.; Amoscato, A. A.; Osipov, A. N.; Belikova, N. A.; Kapralov, A. A.; Kini, V. *Nat. Chem. Biol.* **2005**, *1*, 223−232.
(27) Kagan, V. E.; Bayır, H. A.; Belikova, N. A.; Kapralov, O.; Tyurina, Y. Y.; Tyurin, V. A.; Jiang, J.; Stoyanovsky, D. A.; Wipf, P.; Kochanek, P. M. *Free Radical Biol. Med.* **2009**, *46*, 1439−1453.
(28) Petrosillo, G.; Ruggiero, F. M.; Paradies, G. *FASEB J.* **2003**, *17*, 2202−2208.
(29) De Kruijff, B.; Cullis, P. *Biochim. Biophys. Acta, Biomembr.* **1980**, *602*, 477−490.
(30) Spooner, P. J.; Watts, A. *Biochemistry* **1991**, *30*, 3871−3879.
(31) Hanske, J.; Toffey, J. R.; Morenz, A. M.; Bonilla, A. J.; Schiavoni, K. H.; Pletneva, E. V. *Proc. Natl. Acad. Sci. U. S. A.* **2012**, *109*, 125−130.
(32) Sinibaldi, F.; Howes, B. D.; Piro, M. C.; Polticelli, F.; Bombelli, C.; Ferri, T.; Coletta, M.; Smulevich, G.; Santucci, R. *JBIC, J. Biol. Inorg. Chem.* **2010**, *15*, 689−700.
(33) Vincent, J. S.; Levin, I. W. *J. Am. Chem. Soc.* **1986**, *108*, 3551−3554.
(34) Choi, S.; Swanson, J. M. *Biophys. Chem.* **1995**, *54*, 271−278.
(35) Fox, C. B.; Myers, G. A.; Harris, J. M. *Appl. Spectrosc.* **2007**, *61*, 465−469.
(36) Fox, C. B.; Uibel, R. H.; Harris, J. M. *J. Phys. Chem. B* **2007**, *111*, 11428−11436.
(37) Kitt, J. P.; Bryce, D. A.; Harris, J. M. *Appl. Spectrosc.* **2016**, *70*, 1165−1175.
(38) Myers, G. A.; Harris, J. M. *Anal. Chem.* **2011**, *83*, 6098−6105.
(39) Hardcastle, C. D.; Harris, J. M. *Anal. Chem.* **2015**, *87*, 7979−7986.
(40) Fox, C. B.; Harris, J. M. *J. Raman Spectrosc.* **2010**, *41*, 498−507.
(41) Hu, S.; Morris, I. K.; Singh, J. P.; Smith, K. M.; Spiro, T. G. *J. Am. Chem. Soc.* **1993**, *115*, 12446−12458.
(42) Spiro, T. G.; Smulevich, G.; Su, C. *Biochemistry* **1990**, *29*, 4497−4508.
(43) Cherney, D. P.; Conboy, J. C.; Harris, J. M. *Anal. Chem.* **2003**, *75*, 6621−6628.
(44) Cherney, D. P.; Bridges, T. E.; Harris, J. M. *Anal. Chem.* **2004**, *76*, 4920−4928.
(45) Lawton, W. H.; Sylvestre, E. A. *Technometrics* **1971**, *13*, 617−633.
(46) Malinowski, E. R. *Factor analysis in chemistry*; Wiley: New York, 2002.
(47) Kütt, A.; Rodima, T.; Saame, J.; Raamat, E.; Mäemets, V.; Kaljurand, I.; Koppel, I. A.; Garlyauskayte, R. Y.; Yagupolskii, Y. L.; Yagupolskii, L. M.; Bernhardt, E.; Willner, H.; Leito, I. *J. Org. Chem.* **2011**, *76*, 391−395.
(48) Schaefer, J. J.; Ma, C.; Harris, J. M. *Anal. Chem.* **2012**, *84*, 9505−9512.
(49) MacDonald, R. C.; MacDonald, R. I.; Menco, B. P. M.; Takeshita, K.; Subbarao, N. K.; Hu, L.-r. *Biochim. Biophys. Acta, Biomembr.* **1991**, *1061*, 297−303.
(50) Kitt, J. P.; Harris, J. M. *Anal. Chem.* **2014**, *86*, 1719−1725.
(51) Houlne, M. P.; Sjostrom, C. M.; Uibel, R. H.; Kleimeyer, J. A.; Harris, J. M. *Anal. Chem.* **2002**, *74*, 4311−4319.
(52) Williams, K. P. J.; Pitt, G. D.; Batchelder, D. N.; Kip, B. J. *Appl. Spectrosc.* **1994**, *48*, 232−235.
(53) Rygula, A.; Majzner, K.; Marzec, K.; Kaczor, A.; Pilarczyk, M.; Baranska, M. *J. Raman Spectrosc.* **2013**, *44*, 1061−1076.
(54) Schultz, Z. D.; Levin, I. W. *Annu. Rev. Anal. Chem.* **2011**, *4*, 343−366.
(55) Pelton, J. T.; McLean, L. R. *Anal. Biochem.* **2000**, *277*, 167−176.
(56) Balakrishnan, G.; Hu, Y.; Oyerinde, O. F.; Su, J.; Groves, J. T.; Spiro, T. G. *J. Am. Chem. Soc.* **2007**, *129*, 504−505.
(57) Pandiscia, L. A.; Schweitzer-Stenner, R. *J. Phys. Chem. B* **2015**, *119*, 1334−1349.
(58) Takahashi, S.; Ogura, T.; Shinzawa-Itoh, K.; Yoshikawa, S.; Kitagawa, T. *Biochemistry* **1993**, *32*, 3664−3670.
(59) Yu, N.; Nie, S.; Chang, C. In *12th International Conference on Raman Spectroscopy*; Durig, J., Sullivan, J., Eds.; Wiley-Blackwell: Hoboken, NJ, 1990; pp 902−903.
(60) Orendorff, C. J.; Ducey, M. W.; Pemberton, J. E. *J. Phys. Chem. A* **2002**, *106*, 6991−6998.
(61) Lippert, J.; Peticolas, W. *Biochim. Biophys. Acta, Biomembr.* **1972**, *282*, 8−17.

DOI: 10.1021/jacs.7b00238
J. Am. Chem. Soc. 2017, 139, 3851−3860

(62) Czamara, K.; Majzner, K.; Pacia, M.; Kochan, K.; Kaczor, A.; Baranska, M. *J. Raman Spectrosc.* **2015**, *46*, 4−20.
(63) Pfefferkorn, C. M.; Jiang, Z.; Lee, J. C. *Biochim. Biophys. Acta, Biomembr.* **2012**, *1818*, 162−171.
(64) Swaney, J. B. *J. Biol. Chem.* **1980**, *255*, 8791−8797.
(65) Sorice, M.; Manganelli, V.; Matarrese, P.; Tinari, A.; Misasi, R.; Malorni, W.; Garofalo, T. *FEBS Lett.* **2009**, *583*, 2447−2450.
(66) Postlethwaite, J.; Ong, K.; Pickett, D. *Can. J. Chem. Eng.* **1972**, *50*, 245−247.
(67) Antonov, V. F.; Puchkov, M. N.; Korepanova, E. A.; Nemchenko, O. Y.; Borodulin, V. *Eur. Biophys. J.* **2014**, *43*, 469−476.

DOI: 10.1021/jacs.7b00238
J. Am. Chem. Soc. 2017, 139, 3851−3860